Journal of Nuclear and Radiochemical Sciences, Vol. 21, pp. 15-27, 2021

Articles

Phase transformation of mixed lanthanide oxides in an aqueous solution

Md. Moniruzzaman*[1], Taishi Kobayashi*[2], Takayuki Sasaki

Department of Nuclear Engineering, Kyoto University, Kyotodaigaku-katsura, Nishikyo-ku, Kyoto 615-8540, Japan

Received March 15, 2021; Accepted May 10, 2021; Published online May 26, 2021

Binary and ternary mixed lanthanide oxides including $(La,Nd)_2O_3$, $(La,Eu)_2O_3$, $(Eu,Tm)_2O_3$, $(La,Nd,Eu)_2O_3$, and $(La,Eu,Tm)_2O_3$ were synthesized at 1000 °C for 4 h, followed by characterization using X-ray diffraction (XRD) techniques before and after contact with an aqueous solution at neutral pH and 60 °C for 4 weeks. The XRD patterns of the mixed oxides confirmed a tendency to form oxide or hydroxide solid solutions depending on their mixing ratios. A complete solid solution of $(La,Nd)_2O_3$ underwent transformation to $(La,Nd)(OH)_3$, while the separated La_2O_3 + Nd_2O_3 were converted to $La(OH)_3$ + $Nd(OH)_3$. A similar trend was observed for $(La,Eu)_2O_3$, while $(Eu,Tm)_2O_3$ resulted in separate $Eu(OH)_3$ and Tm_2O_3 after contact with an aqueous solution because of the resistance of Tm_2O_3 to the hydration reaction. The formation of ternary oxide solid solutions and their transformation in an aqueous solution could be satisfactorily explained by the trends observed for binary mixed lanthanides.

1. Introduction

The thermodynamic properties of actinide and lanthanide elements play important roles in the context of nuclear technology. In particular, lanthanide fission products are known to accumulate in the nuclear fuel and exist as oxides that may form a solid solution with a UO_2 matrix.[1,2] For safe treatment and subsequent disposal of spent nuclear fuel, the solubility of such UO_2-based oxide solid solutions is a key factor to reliably predict the migration behavior of radionuclides under disposal conditions. Although a number of studies have investigated the structure, stability, and solubility behavior of these multi-component solid phases, we focused on exploring the thermodynamic properties of single-, binary-, and ternary-component solid phases to better understand those of multi-component solid phases. Since decay heat of the radioactive waste is transferred to groundwater aquifers through surrounding engineered and geological barrier systems in the repositories,[3,4] the present study investigated binary and ternary mixed lanthanide oxides of the $(L_1,L_2)_2O_3$ and $(L_1,L_2,L_3)_2O_3$ type after aging at an elevated temperature to define their structures and stabilities in aqueous systems.

Numerous studies have been conducted that examined the structure, stability, and solubility behavior of pure lanthanide oxides, as described in comprehensive reviews of literature data.[5,6] Moreover, many reports detailed the synthetic methods for the preparation of binary mixed lanthanide oxides, including their solid solutions, and investigated their structures for the development of functional materials.[7–16] The ionic radius of lanthanides plays an important role in the formation of mixed lanthanide oxides. Heiba et al. synthesized $(Er_{1-u}Gd_u)_2O_3$ powder samples with various mixing proportions of Gd and Er and confirmed the formation of complete solid solutions for all mixing ratios.[9] On the other hand, Hirsch et al. showed the formation of separated solid solutions for Nd_2O_3:Lu_2O_3 synthesized at 1350–1500 °C, namely, a Lu- and Nd-dominated solid solution with a cubic $(Lu_{1-x}Nd_xO_3)$ and hexagonal $(Nd_{1-x}Lu_xO_3)$ structure, respectively.[10] In contrast to the abundant knowledge on the structures of synthetic mixed lanthanide oxides, no studies have investigated their solid phase transformation occurring upon contacting aqueous solutions. For a comprehensive model of the radionuclide migration behavior during radioactive waste management, the thermodynamic properties of lanthanides in aqueous systems need to be clarified.[17,18]

Recently, we've examined pure oxides of light, medium, and heavy lanthanides (La_2O_3, Eu_2O_3, and Tm_2O_3) after being in contact with aqueous sample solutions, and revealed that La_2O_3 was converted to $La(OH)_3$ under neutral to alkaline pH conditions at 25 °C.[19] On the other hand, Eu_2O_3 remained stable at 25 °C and underwent transformation to $Eu(OH)_3$ only after aging at 90 °C, while Tm_2O_3 was stable even after aging at 90 °C.[19] This study deals with binary and ternary mixed lanthanide oxides before and after contact with an aqueous solution. Since the solid phase transformation tendency upon contacting aqueous solutions differs from lighter to heavier lanthanides, binary [$(La,Nd)_2O_3$, $(La,Eu)_2O_3$, and $(Eu,Tm)_2O_3$] and ternary [$(La,Nd,Eu)_2O_3$ and $(La,Eu,Tm)_2O_3$] systems were selected and synthesized at various mixing ratios. The mixed oxides were then immersed in an aqueous solution within the neutral pH region at 60 °C for 4 weeks. The aging temperature of 60 °C was used as a moderate elevated temperature condition in the repository due to the decay heat emission from the radioactive waste.[3] The solid phases were examined before and after immersion by powder X-ray diffraction (XRD), and the phase transformation of mixed lanthanide oxides was analyzed with the aid of the obtained lattice parameters.

2. Experimental

2.1 Materials. Reagent grade sodium perchlorate monohydrate ($NaClO_4 \cdot H_2O$, 98%), nitric acid (HNO_3, 60 %), perchloric acid ($HClO_4$, 60%), sodium hydroxide (NaOH, 97%), and polyvinyl alcohol (PVA, 3,500, 78% hydrolyzed) were purchased from Wako Pure Chem. HEPES ($C_8H_{18}N_2O_4S$, 99.0%, Dojindo) was used to adjust the pH of the sample solutions to a neutral pH region. Lanthanum oxide (La_2O_3, 99.99%), neodymium oxide (Nd_2O_3, 99.9%), europium oxide (Eu_2O_3, 99.9%), and thulium oxide (Tm_2O_3, 99.9%) were purchased

*[1]Corresponding author 1: Email: mohammad.moniruzzaman.23c@st.kyoto-u.ac.jp
*[2]Corresponding author 2: Email: kobayashi@nucleng.kyoto-u.ac.jp

Published on Web 05/26/2021

from Wako Pure Chem. Deionized purified water (Milli-Q, Millipore) was used to prepare all the solutions. The synthesis of the solid phases and preparation of the sample solutions were performed under atmospheric pressure at 25 °C. The pH_c values of the sample solutions were measured using a pH meter (D-72, Horiba Ltd.) with a combined glass electrode (9615-10D, Horiba Ltd.). The reference electrode was filled with 3.6 M NaCl and 0.41 M $NaClO_4$ (Wako Pure Chem.) instead of 3.3 M KCl to prevent precipitation of $KClO_4$ at the junction of the electrode and sample solutions. The electrode was calibrated against standard $HClO_4$ and NaOH solutions (pH_c 1, 2, 3, 11, 12, and 13; Wako Pure Chem.) at I = 0.1 M using $NaClO_4$ at 25 °C to correct the experimentally measured pH_{exp} to the pH_c values.

2.2 Synthesis of binary and ternary mixed oxide. Three types of binary mixed oxides, i.e., $(La,Nd)_2O_3$, $(La,Eu)_2O_3$, and $(Eu,Tm)_2O_3$, and two types of ternary mixed oxides, i.e., $(La,Nd,Eu)_2O_3$ and $(La,Eu,Tm)_2O_3$, were synthesized by using a polymeric steric entrapment method.[20,21] An appropriate amount of PVA was dissolved in Milli-Q water to obtain a 5 wt% PVA stock solution. Ln (Ln = La, Nd, Eu, and Tm) nitrate stock solutions with a concentration of [Ln] = 0.3 M were prepared by dissolving La_2O_3, Nd_2O_3, Eu_2O_3, or Tm_2O_3(cr) in nitric acid. For the preparation of $(La,Nd)_2O_3$, aliquots of La and Nd stock solutions were mixed at molar ratios of La:Nd = 1:9, 3:7, 4:6, 5:5, 7:3, and 9:1, and an equivalent molar amount of PVA stock solution was then added to the mixed Ln solutions. The resulting solutions were stirred for 1 h using a magnetic stirrer and heated at 200 °C for approximately 2 h. After drying, the solids were crushed in a mortar, and further heated at 1000 °C for 4 h using a muffle furnace (FO-100, Yamato Scientific Co.). Mixed oxides $(La,Eu)_2O_3$ and $(Eu,Tm)_2O_3$ were prepared in a similar manner. As reference, oxide mixtures including La_2O_3+Nd_2O_3, La_2O_3+Eu_2O_3, and Eu_2O_3+Tm_2O_3 were prepared without heating by mixing each oxide at the same weight ratio and grinding for 10 min.

For the preparation of $(La,Nd,Eu)_2O_3$, aliquots of La, Nd, and Eu stock solutions were mixed at molar ratios of La:Nd:Eu = 4.75:4.75:0.5, 4.5:4.5:1.0, and 3.5:3.5:3.0. An equivalent molar amount of PVA stock solution was then added to the mixed solutions, and the ternary mixed oxides were obtained using a similar procedure as that used for the synthesis of binary mixed oxides. For the preparation of $(La,Eu,Tm)_2O_3$, the molar ratios of La, Eu, and Tm stock solutions were 0.5:4.75:4.75, 1.0:4.5:4.5, 3.0:3.5:3.5, and 4.5:4.5:1.0. For comparison, mixtures of pure oxides such as La_2O_3+Nd_2O_3+Eu_2O_3 and La_2O_3+Eu_2O_3+Tm_2O_3 were also prepared without heating.

The synthesized mixed oxides and prepared mixtures of pure oxides were analyzed using XRD (Miniflex, RIGAKU) with Cu-Kα (λ = 0.154 nm) in the scattering angle range of 2θ = 10–60° at a scan rate of 5°/min. To determine the chemical composition of the solid phases, small portions of the selected solid phases were completely dissolved in concentrated nitric acid, and the Ln concentration was determined by ICP-MS (ELAN DRC II, PerkinElmer) to calculate the molar ratio of Ln included in each solid phase. The chemical composition of the solid phases agreed well with the mixing ratio of the stock solutions used for sample preparation.

2.3 Immersion experiment. For the immersion experiment, 80 mL of a 0.1 M $NaClO_4$ solution containing 0.01 M HEPES as pH buffer was prepared in sample bottles, and the pH_c was adjusted to pH = 8.2 using 0.1 M $HClO_4$ and 0.1 M NaOH. As an initial solid phase, approximately each 130 mg of synthesized oxide solid solution or mixture of pure oxides was then placed in the sample bottles. The maximum Ln concentration would reach about 0.01 M in each bottle if the added solid phase was completely dissolved. Subsequently, the caps of the sample bottles were tightly closed, and the sample bottles were placed in a temperature chamber (ETTAS E0450B, AS ONE co.) at the controlled aging temperature (T_{age}) of 60 °C. The bottles were occasionally shaken by hand for a few minutes during aging up to 4 weeks. After aging at 60 °C, the sample bottles were removed from the temperature chamber and cooled to 25 °C for a few days. The pH_c of the sample solutions was within the 8.2 ± 0.3 range, and the solid phases were separated by centrifugation at 5,000 rpm (H-103N, Kokusan) for 5 min and dried in a vacuum desiccator. The diffraction patterns of the solid phases were recorded by XRD.

3. Results and discussion

3.1 Characterization of the synthesized binary and ternary mixed oxides. Figure 1 shows the XRD patterns of the synthesized $(La,Nd)_2O_3$ mixed oxides at different mixing ratios of La and Nd stock solutions ranging from La:Nd = 9:1 to 1:9 during sample preparation, together with those of pure La_2O_3 and Nd_2O_3. As observed in the XRD patterns, the peaks corresponding to La_2O_3 slightly shifted towards the right side with increasing mixing ratio of Nd to pure Nd_2O_3. It is note that the observed peak positions of Nd_2O_3 were slightly higher than those of the reference (Nd_2O_3: ICSD No. 26867). The XRD pattern of the 5:5 mixture of pure La_2O_3 and Nd_2O_3 without any treatment is also presented in Figure 1. Separated peaks were observed for La_2O_3 and Nd_2O_3, indicating that the resolution of the present measurement was sufficient to distinguish the peaks of two different pure oxides. Therefore, it was assumed that complete solid solutions of $(La,Nd)_2O_3$ were formed using the polymeric steric entrapment method at 1000 °C.

Figure 2 shows the XRD patterns of the synthesized $(La,Eu)_2O_3$ at different mixing ratios of La and Eu stock solutions ranging from La:Eu = 9:1 to 1:9, together with those of pure La_2O_3, Eu_2O_3, and their mixture without heating. In contrast to $(La,Nd)_2O_3$, the peaks corresponding to both cubic and monoclinic Eu_2O_3 disappeared only at an La:Eu mixing ratio of 9:1, and separately appeared at an La:Eu mixing ratio of 7:3 to pure Eu_2O_3, suggesting that the solid solution limit of Eu to La_2O_3 was between 10 and 30% in molar ratio under the investigated conditions. On the other hand, the solid solution limit of La to Eu_2O_3 was considered to be less than 10% in molar

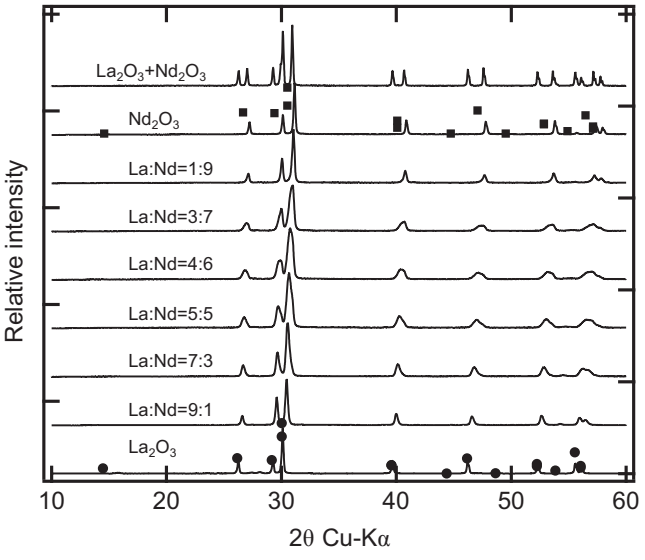

Figure 1. XRD patterns of the synthesized $(La,Nd)_2O_3$ at different mixing ratios ranging from La:Nd =9:1 to 1:9, along with that of a mixture of La_2O_3 and Nd_2O_3 without heating. XRD patterns of pure La_2O_3 and Nd_2O_3 and their reference peak positions (●: La_2O_3: ICSD No. 1010278, ■: Nd_2O_3: ICSD No. 26867) are also presented for comparison.

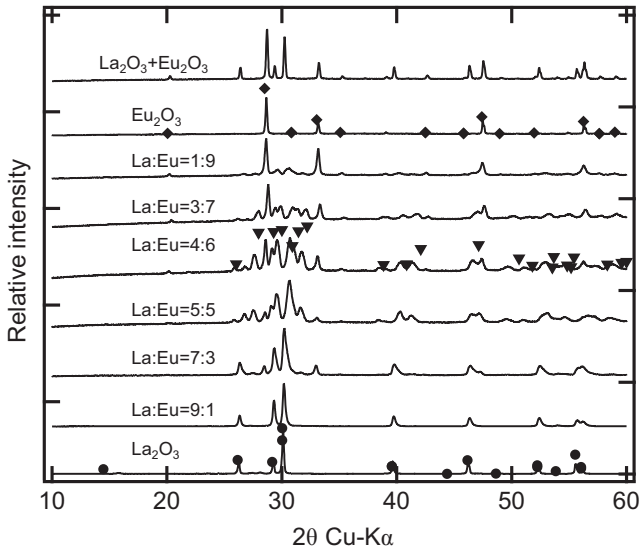

Figure 2. XRD patterns of the synthesized $(La,Eu)_2O_3$ at different mixing ratios ranging from La:Eu = 9:1 to 1:9, along with that of a mixture of La_2O_3 and Eu_2O_3 without heating. XRD patterns of pure La_2O_3 and Eu_2O_3 and their reference peak positions (●: La_2O_3: ICSD No. 1010278, ♦: Eu_2O_3 (cubic): ICSD No. 27997, ▼: Eu_2O_3 (monoclinic): ICSD No. 8066) are also presented for comparison.

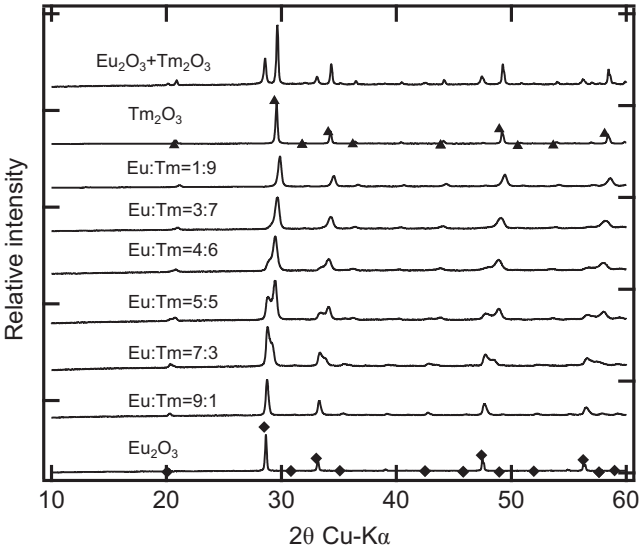

Figure 3. XRD patterns of the synthesized $(Eu,Tm)_2O_3$ at different mixing ratios ranging from Eu:Tm = 9:1 to 1:9, along with that of a mixture of Eu_2O_3 and Tm_2O_3 without heating. XRD patterns of pure Eu_2O_3 and Tm_2O_3 and their reference peak positions (♦: Eu_2O_3: ICSD No. 27997, ▲: Tm_2O_3: ICSD No. 33657) are also presented for comparison.

ratio, as a small peak at 29.8° corresponding to La_2O_3 was already found in $(La,Eu)_2O_3$ at a La:Eu mixing ratio of 1:9.

It was reported that Eu_2O_3 exhibits a stable cubic phase up to approximately 620 °C that transforms into a monoclinic phase.[22,23] The cubic phase observed in the XRD pattern of pure Eu_2O_3 in the present study may have been formed during furnace cooling after heating at 1000 °C. It is interesting to note that diffraction peaks corresponding to monoclinic Eu_2O_3 were observed in the solid phases with La:Eu mixing ratios of 3:7, 4:6, and 5:5. In previous studies, the inclusion of another rare earth oxide such as Y_2O_3 to Eu_2O_3 was observed to affect the phase change temperature.[23] The appearance of the monoclinic phase for $(La,Eu)_2O_3$ at certain mixing ratios shown in Figure 2 can be attributed to the inclusion of La in the Eu_2O_3 phase.

The XRD patterns of the synthesized $(Eu,Tm)_2O_3$ at different mixing ratios of Eu and Tm stock solutions ranging from Eu:Tm = 9:1 to 1:9 are shown in Figure 3, together with those of pure Eu_2O_3, Tm_2O_3, and their mixture without heating. At an Eu:Tm mixing ratio of 9:1, the peaks corresponding to Tm_2O_3 were not observed in the corresponding XRD pattern, suggesting the formation of a $(Eu,Tm)_2O_3$ solid solution, while a small shoulder peak was observed for Eu:Tm = 7:3. In contrast, the peaks of Eu_2O_3 did not appear at Eu:Tm = 1:9 and 3:7, while the peaks corresponding to Tm_2O_3 slightly shifted towards the left side, indicating that the solid solution limit of Eu to Tm_2O_3 was higher than that of Tm to Eu_2O_3. At Eu:Tm ratios of 5:5 to 7:3, separated peaks corresponding to both cubic Eu_2O_3 and Tm_2O_3 were observed in the diffraction patterns. As described above, the cubic phase of Eu_2O_3 was considered to derive from its monoclinic phase during furnace cooling, while the cubic phase of Tm_2O_3 was stable up to approximately 2000 °C.[22] This may be the reason for the separation of the diffraction peaks of the Eu_2O_3 and Tm_2O_3 cubic phases.

Figure 4 shows the XRD patterns of the synthesized $(La,Nd,Eu)_2O_3$ at different La:Nd:Eu mixing ratios of 4.75:4.75:0.5, 4.5:4.5:1.0, and 3.5:3.5:3.0, along with a mixture of pure oxides (La_2O_3+Nd_2O_3+Eu_2O_3) without any heat treatment. For the binary systems, the synthesized $(La,Nd)_2O_3$ was a complete solid solution, while $(La,Eu)_2O_3$ showed trigonal, cubic, and monoclinic phases depending on the La and Eu

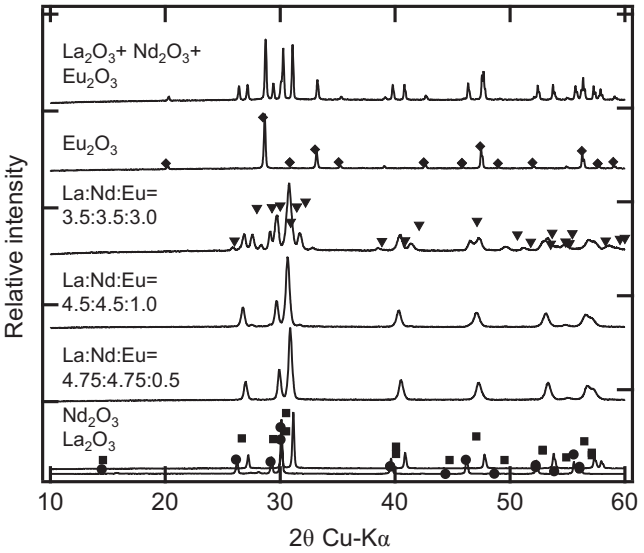

Figure 4. XRD patterns of the synthesized $(La,Nd,Eu)_2O_3$ at different mixing ratios as La:Nd:Eu = 4.75:4.75:0.5, 4.5:4.5:1.0 and 3.5:3.5:3.0 along with that of a mixture of La_2O_3, Nd_2O_3, and Eu_2O_3 without heating. The reference peak positions (●: La_2O_3: ICSD No. 1010278, ■: Nd_2O_3: ICSD No. 26867, ♦:Eu_2O_3: ICSD No. 27997,▼: Eu_2O_3: ICSD No. 8056) are presented for comparison.

mixing ratios. In the case of ternary systems with a low Eu mixing ratio such as La:Nd:Eu = 4.75:4.75:0.5 and 4.5:4.5:1.0, a single phase corresponding to the trigonal phase was observed. The intermediate peak positions between those of pure La_2O_3 and Nd_2O_3 suggested the formation of a solid solution, which agrees with the observation for the $(La,Nd)_2O_3$ binary system. As shown in **Figure 2** for $(La,Eu)_2O_3$ binary systems, the inclusion of 30% Eu resulted in the appearance of Eu_2O_3 with cubic and monoclinic phases, which was also found in the XRD patterns of the ternary system with La:Nd:Eu = 3.5:3.5:3.0.

Figure 5 shows the XRD patterns of the synthesized $(La,Eu,Tm)_2O_3$ at different mixing ratios including La:Eu:Tm = 0.5:4.75:4.75, 1.0:4.5:4.5, 3.0:3.5:3.5, and 4.5:4.5:1.0, along with a mixture of pure oxides (La_2O_3+Eu_2O_3+Tm_2O_3) without any heat treatment. For the $(Eu,Tm)_2O_3$ binary system, separated

cubic phases occurred at a Eu:Tm mixing ratio of 5:5. Similarly, peaks corresponding to cubic Eu_2O_3 and Tm_2O_3 were observed separately at all mixing ratios for the investigated ternary systems. The peaks corresponding to trigonal La_2O_3 were not confirmed for lower La inclusions at La:Eu:Tm mixing ratios of 0.5:4.75:4.75 and 1.0:4.5:4:5 as well as those appearing at La:Eu:Tm = 3.0:3.5:3.5 and 4.5:4.5:1.0, although these peaks were observed for 10% La inclusion in the binary $(La,Eu)_2O_3$ systems. At La:Eu:Tm = 3.0:3.5:3.5 and 4.5:4.5:1.0, peaks corresponding to monoclinic Eu_2O_3 were found, which

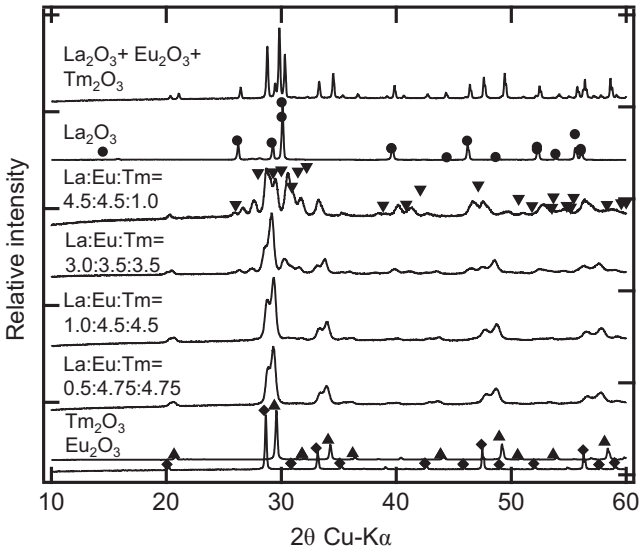

Figure 5. XRD patterns of the synthesized $(La,Eu,Tm)_2O_3$ at different mixing ratios as La:Eu:Tm = 0.5:4.75:4.75, 1.0:4.5:4.5, 3.0:3.5:3.5 and 4.5:4.5:1.0 along with that of a mixture of La_2O_3, Eu_2O_3, and Tm_2O_3 without heating. The reference peak positions (●: La_2O_3: ICSD No. 1010278, ♦: Eu_2O_3: ICSD No. 27997, ▼: Eu_2O_3 ICSD No. 8056, ▲: Tm_2O_3: ICSD No. 33657) are presented for comparison.

agreed with the observations for the $(La,Eu)_2O_3$ binary system at La:Eu = 5:5. Thus, the trends of the XRD patterns for the $(La,Nd,Eu)_2O_3$ and $(La,Eu,Tm)_2O_3$ ternary solid phases could be suitably explained based on the combination of those of the binary systems.

For further analysis, the lattice parameters of the synthesized solid solutions were obtained from Rietveld refinement, as summarized in Tables A1-A5 in the Appendix. Figure 6a illustrates the obtained lattice parameter *a* and weight fraction of the trigonal phase found in the binary and ternary systems as a function of the La mixing ratio. As pure La_2O_3 and Nd_2O_3 possess the same crystal structure of the trigonal phase with a (P-3m1) space group, the replacement of Nd with La continuously increased the lattice parameter *a*, which could be attributed to the smaller radius of the Nd ion compared with that of the La ion. The lattice parameter of the trigonal phase found in $(La,Eu)_2O_3$ slightly decreased compared to that of pure La_2O_3 with decreasing La mixing ratios. The low values observed at La ratios of 0.3, 0.4, and 0.5 are possibly due to the appearance of the Eu_2O_3 monoclinic phase (C2/m) under these conditions. As shown in Figure 6b, La hardly incorporated into the Eu_2O_3 cubic phase (Ia-3), but it did into the monoclinic phase. The La ratio of the $(La,Eu)_2O_3$ trigonal phase can therefore be expected to be lower than that of the mixing La ratio during sample preparation. The lattice parameters of $(La,Nd,Eu)_2O_3$ plotted in Figure 6a agreed well with the trend observed for $(La,Nd)_2O_3$, which was likely due to the limited amount of Eu. In the case of the ternary $(La,Eu,Tm)_2O_3$ system, Eu incorporated into Tm_2O_3, as shown in Figure 6b; consequently, the Eu ratio decreased, while the La ratio increased in the $(La,Eu)_2O_3$ trigonal phase. This may compensate for the decrease in the La ratio due to the appearance of the monoclinic phase.

The lattice parameter of the cubic phase (Ia-3) of $(La,Eu)_2O_3$ shown in Figure 6b was slightly larger than that of pure Eu_2O_3 at an Eu ratio of 0.9, while being almost constant at a lower Eu

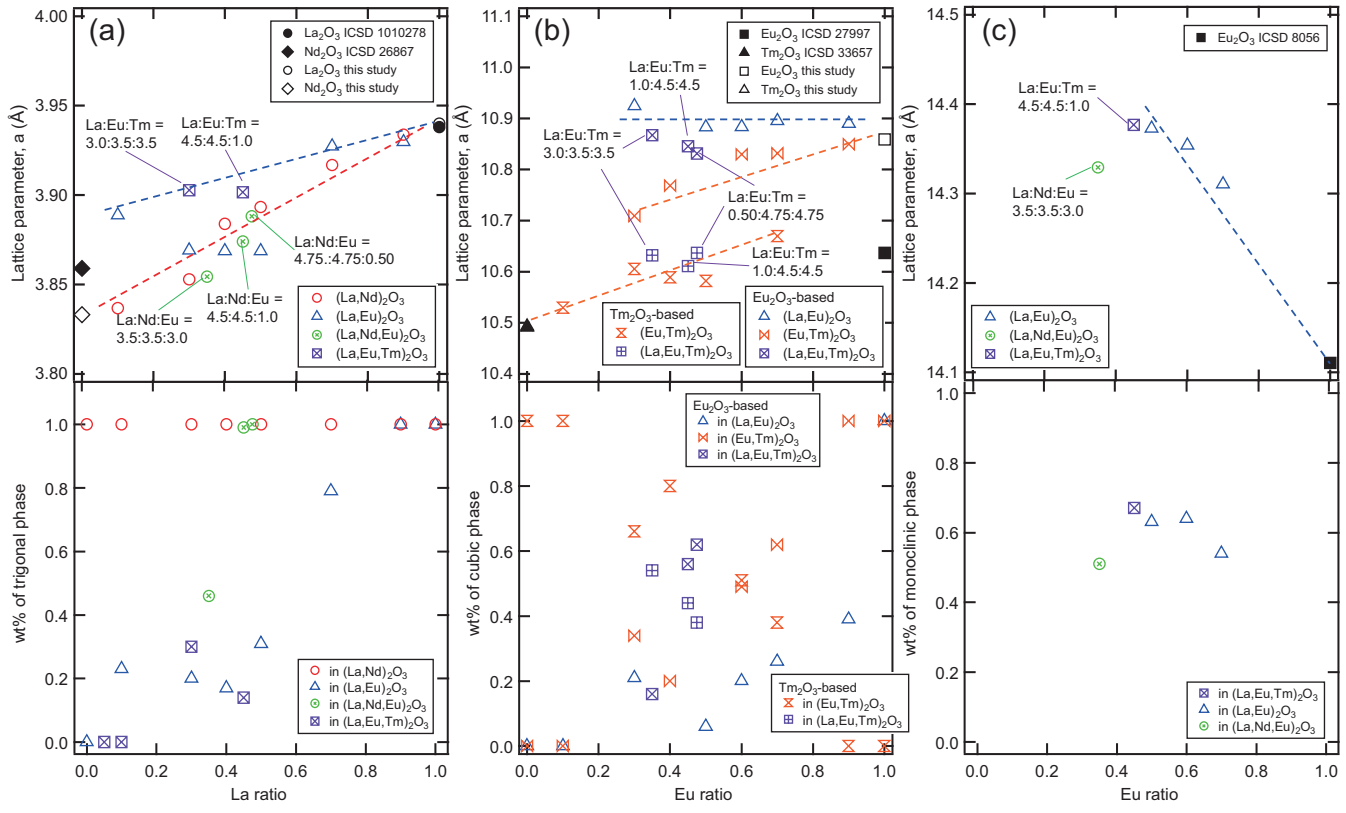

Figure 6. Lattice parameter *a* (upper) and weight fraction (lower) of the synthesized (a) trigonal phase (b) cubic phase, and (c) monoclinic phase of the binary and ternary systems as a function of the molar mixing ratio. Broken lines in the figures represent the eye guides to show the trend for the binary systems.

ratio. As observed in the XRD patterns, the inclusion of 10% La exceeded the solid solution limit of La into Eu_2O_3, supporting the observed trend of the lattice parameters. For $(Eu,Tm)_2O_3$, two cubic phases, i.e., an Eu_2O_3- and Tm_2O_3-based solid solution, were observed. As shown in Figure 6b, the lattice parameters for both Eu_2O_3- and Tm_2O_3-based cubic phases slightly increased with increasing Eu ratios. Upon heating at 1000 °C, Eu_2O_3 can exist as a monoclinic phase and be converted to the cubic phase upon furnace cooling. In contrast to La, the co-existing Tm seemed to have no significant effect on maintaining the monoclinic phase, while potentially causing some scattering in the increasing lattice parameter trend. The lattice parameters of the Eu_2O_3-based cubic phase of ternary $(La,Eu,Tm)_2O_3$ were plotted between those of $(La,Eu)_2O_3$ and $(Eu,Tm)_2O_3$, while those of the Tm_2O_3-based cubic phase were rather close to those of $(Eu,Tm)_2O_3$. As shown in Figure 6c, La seemed to be easily incorporated into the Eu_2O_3 monoclinic phase, which was converted to the Eu_2O_3 cubic phase. This could be why the lattice parameters of the Eu_2O_3-based cubic phase of $(La,Eu,Tm)_2O_3$ showed higher values than those of $(Eu,Tm)_2O_3$.

The lattice parameter *a* and weight fraction of the monoclinic phase (C2/m) are shown in Figugre 6c, respectively. As discussed above, the lattice parameters of the binary and ternary systems were larger than those of the pure Eu_2O_3 monoclinic phase, suggesting a relatively good incorporation of La into the Eu_2O_3 monoclinic phase.

3.2 Characterization of the solid phases after contact with an aqueous solution. The XRD patterns of the solid phases after contact of the synthesized $(La,Nd)_2O_3$ with an aqueous sample solution at 60 °C for 4 weeks are presented in Figure 7. The peaks corresponding to the $(La,Nd)_2O_3$ solid solution shown in Figure 1 disappeared, and new peaks continuously shifted rightward in correspondence of mixing ratios of La and Nd stock solutions varying from La:Nd = 9:1 to 1:9. In the previous studies, it was described that pure La_2O_3 and Nd_2O_3 are converted to $La(OH)_3$ and $Nd(OH)_3$ upon contact with aqueous sample solutions.[18,19,24] By comparing the peak positions in Figure 7 to those for $La(OH)_3$ and $Nd(OH)_3$, it was assumed that the complete solid solution of $(La,Nd)_2O_3$ was transformed into a complete solid solution of $(La,Nd)(OH)_3$. However, it is interesting to note that the mixture of La_2O_3 and Nd_2O_3 without any heat treatment resulted in the formation of $La(OH)_3$ and $Nd(OH)_3$, respectively, as shown in Figure 7.

Figure 8 shows the XRD patterns of the solid phases after contact of the synthesized $(La,Eu)_2O_3$ with an aqueous solution. Depending on the mixing ratios of the La and Eu stock solutions, the synthesized $(La,Eu)_2O_3$ was found to occur as a mixture of an La_2O_3- and Eu_2O_3-based solid solution before contacting aqueous phase as shown in Figure 2. However, after aging in the sample solutions, the peaks corresponding to both oxide-based solid solutions disappeared, and new peaks continuously shifted rightward with the La:Eu ratio varying from 9:1 to 1:9. It was therefore assumed that for the synthesized $(La,Eu)_2O_3$, the mixture of the two oxide-based solid solutions was transformed to a complete solid solution of $(La,Eu)(OH)_3$. In the pure system, Eu_2O_3 remained stable in aqueous solution at 25 °C and was converted to $Eu(OH)_3$ after aging in aqueous solution at 90 °C.[19] Figure 8 shows that the mixture of La_2O_3 and Eu_2O_3 without any heat treatment resulted in the formation of $La(OH)_3$ and $Eu(OH)_3$ after aging at 60 °C. As some of the main peak positions of Eu_2O_3 overlapped those of $La(OH)_3$ and $Eu(OH)_3$, the amount of remaining Eu_2O_3 was determined in the Rietveld refinement and shown in the Table A2. The results suggested that Eu_2O_3 was partly transformed to $Eu(OH)_3$ after aging at 60 °C. Based on the reported thermodynamic constants, the solubility product of $Eu(OH)_3$ was calculated to be slightly lower than that of

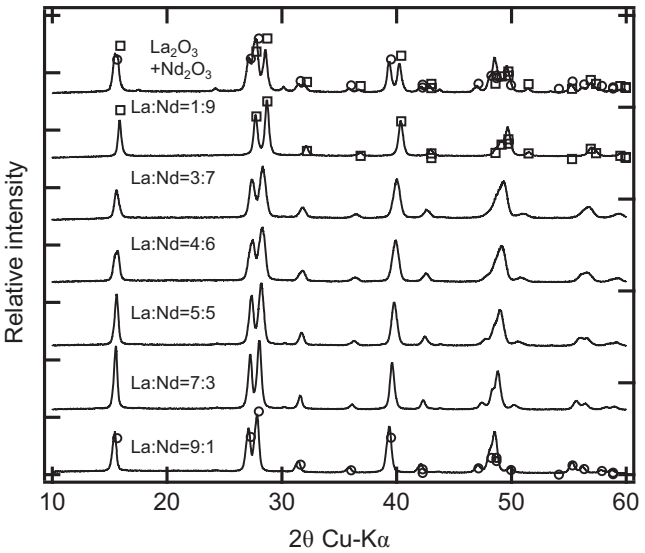

Figure 7. XRD patterns of $(La,Nd)_2O_3$ after contacting the aqueous sample solution at 60 °C for 4 weeks at different mixing ratios ranging from La:Nd = 9:1 to 1:9, along with that of a mixture of La_2O_3 and Nd_2O_3. The reference peak positions ○: $La(OH)_3$ (ICSD No. 31584) and □: $Nd(OH)_3$ (ICSD No. 398) are presented for comparison. The mixture of oxides was identified as $La(OH)_3$+ $Nd(OH)_3$ after the aging period.

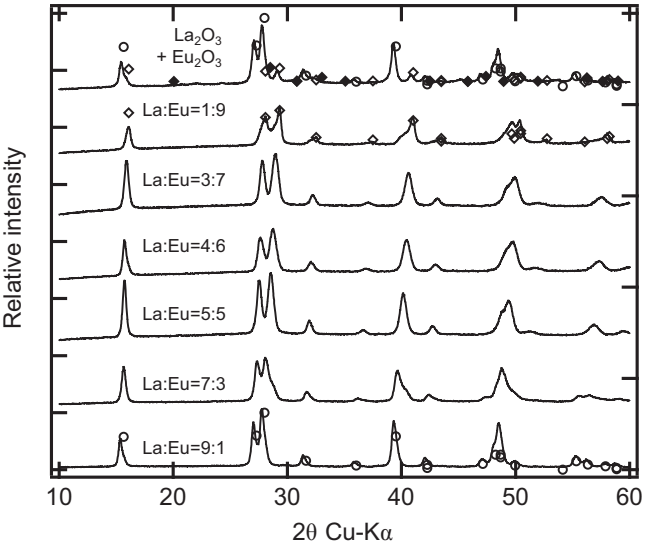

Figure 8. XRD patterns of $(La,Eu)_2O_3$ after contacting the aqueous sample solution at 60°C for 4 weeks at different mixing ratios ranging from La:Eu = 9:1 to 1:9, along with that of a mixture of La_2O_3 and Eu_2O_3. The reference peak positions ○: $La(OH)_3$ (ICSD No. 31584) , ◊: $Eu(OH)_3$ (ICSD No. 200488) and ♦: Eu_2O_3 (ICSD No. 27997) are presented as references. The mixture of oxides was identified as $La(OH)_3$+Eu_2O_3+$Eu(OH)_3$ after the aging period.

Eu_2O_3 at 25 to 90 °C,[5,6,18,19] indicating the transformation of Eu_2O_3 to $Eu(OH)_3$ proceeds thermodynamically via dissolution and reprecipitation. However, in the present study we observed that the solid phases after contact of $(La,Eu)_2O_3$ and La_2O_3+ Eu_2O_3 with the aqueous solution were different from each other as shown in Figure 8. Therefore, the temperature dependences of the transformation of Eu_2O_3 to $Eu(OH)_3$ may not be related in the dissolution and reprecipitation processes.

Figure 9 shows the XRD patterns of the solid phases after contact of the synthesized $(Eu,Tm)_2O_3$ with an aqueous solution. The Tm_2O_3-based solid solution remained stable at Eu:Tm ratios varying from 1:9 to 4:6, after aging in an aqueous sample solution at 60 °C, and no peak due to Eu_2O_3 or $Eu(OH)_3$ was observed. The peaks corresponding to $Eu(OH)_3$ appeared

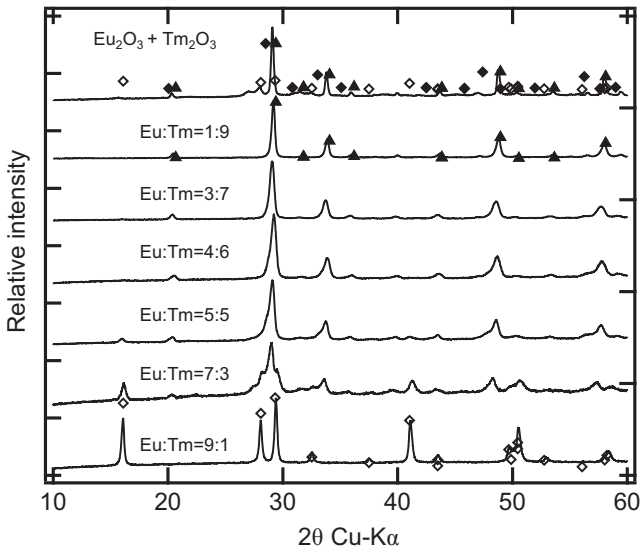

Figure 9. XRD patterns of $(Eu,Tm)_2O_3$ after contacting the aqueous sample solution at 60°C for 4 weeks at different mixing ratios ranging from Eu:Tm = 9:1 to 1:9, along with that of a mixture of Eu_2O_3 and Tm_2O_3. The reference peak positions ◊: $Eu(OH)_3$ (ICSD No. 200488), ♦: Eu_2O_3 (ICSD No. 27997), and ▲: Tm_2O_3 (ICSD No. 33657) are presented for comparison. The mixture of oxides was identified as Eu_2O_3+$Eu(OH)_3$+Tm_2O_3 after the aging period.

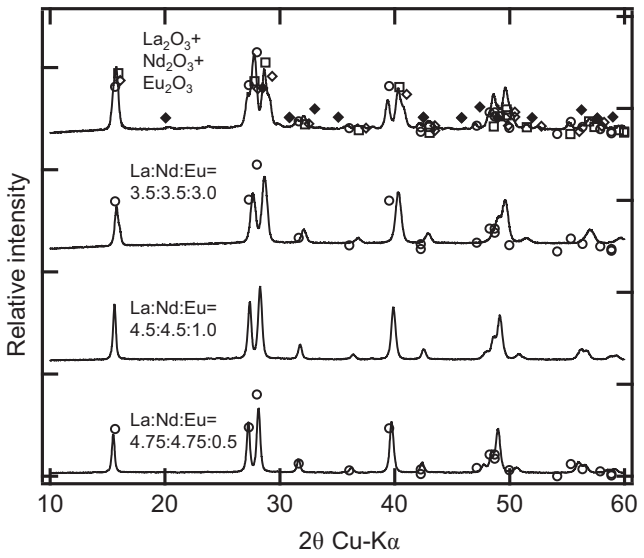

Figure 10. XRD patterns of $(La,Nd,Eu)_2O_3$ after contacting the aqueous sample solution at 60 °C for 4 weeks at different mixing ratios as La:Nd:Eu = 4.75:4.75:0.5, 4.5:4.5:1.0 and 3.5:3.5:3.0 along with that of a mixture of La_2O_3, Nd_2O_3, and Eu_2O_3 without heating. XRD pattern for reference peak positions ○: $La(OH)_3$ (ICSD No. 31584), □: $Nd(OH)_3$ (ICSD No. 398), ◊: $Eu(OH)_3$ (ICSD No. 200488), and ♦: Eu_2O_3 (ICSD No. 27997) are presented for comparison. The mixture of oxides was identified as $La(OH)_3$+$Nd(OH)_3$+$Eu(OH)_3$+Eu_2O_3 after the aging period.

at Eu:Tm = 5:5 to 9:1, supporting the transformation of Eu_2O_3 to $Eu(OH)_3$. At a mixing ratio of Eu:Tm = 9:1, only the peaks of $Eu(OH)_3$ were observed, suggesting that the incorporation of Tm into $Eu(OH)_3$ took place. In Figure 9, the XRD pattern of the solid phase after contact with a mixture of Eu_2O_3 and Tm_2O_3 revealed that Eu_2O_3 partly transformed to $Eu(OH)_3$, while Tm_2O_3 remained stable.

The XRD patterns of the solid phases after contact of the synthesized $(La,Nd,Eu)_2O_3$ with an aqueous sample solution at 60 °C for 4 weeks are presented in Figure 10. Although the peaks corresponding to Eu_2O_3 were separately observed at a 30% Eu mixing ratio before contact with an aqueous solution,

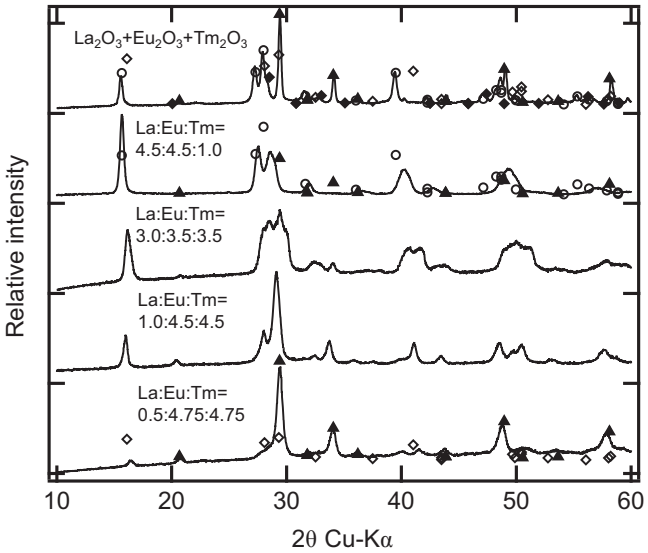

Figure 11. XRD patterns of $(La,Eu,Tm)_2O_3$ after contacting the aqueous sample solution at 60 °C for 4 weeks at different mixing ratios as La:Eu:Tm = 0.5:4.75:4.75, 1.0:4.5:4.5, 3.0:3.5:3.5 and 4.5:4.5:1.0, along with that of a mixture of La_2O_3, Eu_2O_3 and Tm_2O_3 without heating. XRD pattern for reference peak positions ○: $La(OH)_3$ (ICSD No. 31584), ◊: $Eu(OH)_3$ (ICSD No. 200488), ♦: Eu_2O_3 (ICSD No. 27997), and ▲: Tm_2O_3 (ICSD No. 33657) are presented for comparison. The mixture of oxides was identified as $La(OH)_3$+Eu_2O_3+Tm_2O_3 after the aging period.

these peaks disappeared after contact with the aqueous solution. Newly observed peaks with small rightward shifts, i.e. higher 2θ values, depending on the mixing ratios suggested the formation of a single $(La,Nd,Eu)(OH)_3$ solid solution at all mixing ratios. A similar behavior was observed for the binary systems, where $(La,Nd)_2O_3$ and $(La,Eu)_2O_3$ were transformed to complete solid solutions of $(La,Nd)(OH)_3$ and $(La,Eu)(OH)_3$ after contact with an aqueous solution at 60 °C. The mixture of pure La_2O_3, Nd_2O_3, and Eu_2O_3 without heat treatment resulted in the formation of separate hydroxides, i.e., $La(OH)_3$, $Nd(OH)_3$, $Eu(OH)_3$, and Eu_2O_3 after contact with an aqueous solution as shown in Table A4.

Figure 11 shows the XRD patterns of the solid phases after contact of the synthesized $(La,Eu,Tm)_2O_3$ with an aqueous solution at 60 °C for 4 weeks. At an La:Eu:Tm mixing ratio of 0.5:4.75:4.75, the peaks corresponding to the Eu_2O_3 cubic phase disappeared, while those of the Tm_2O_3 cubic phase remained. The newly observed peaks were assigned to the hexagonal phase of $Eu(OH)_3$. As no separated peaks for the $La(OH)_3$ hexagonal phase were confirmed, it was assumed that La was incorporated into the $Eu(OH)_3$ phase to form a solid solution, as observed for the La-Eu binary system. The peaks corresponding to the $(La,Eu)(OH)_3$ hexagonal phase continuously shifted leftward, i.e. lower 2θ values, with increasing La mixing ratios for the ternary system. As observed for the $(Eu,Tm)_2O_3$ binary system after contact with an aqueous solution, the solid solution limit of Tm to $Eu(OH)_3$ fall between 10 and 30%. The peaks of Tm_2O_3 disappeared at an La:Eu:Tm mixing ratio of 4.5:4.5:1.0, indicating that Tm was incorporated into the $(La,Eu)(OH)_3$ hexagonal phase. It is also interesting to note that the mixture of La_2O_3+Eu_2O_3+Tm_2O_3 after contact with an aqueous phase showed a consistent behavior, undergoing transformation into a mixture of $La(OH)_3$, Eu_2O_3, and Tm_2O_3 as shown in Table A5. Since the lattice parameters of $Eu(OH)_3$ were not determined in reasonable ranges due to their limited contributions, $Eu(OH)_3$ was excluded in the analysis.

The lattice parameters for the solid phases after contact of the sample solutions are summarized in Tables A1-A5 and plotted in Figure 12 as a function of the mixing ratio. Figure

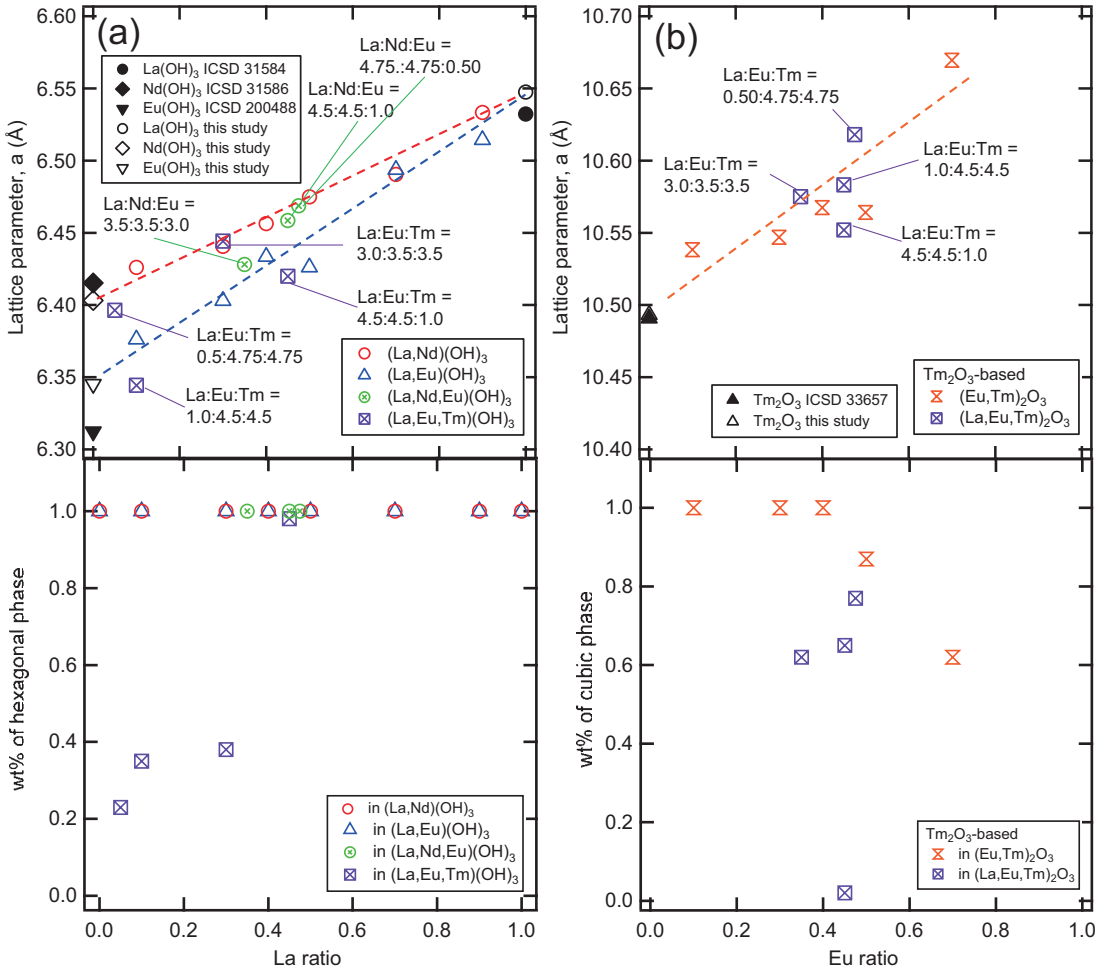

Figure 12. Lattice parameter *a* (upper) and weight fraction (lower) of the synthesized (a) hexagonal phase and (b) cubic phase of the binary and ternary systems as a function of the molar mixing ratios. Broken lines in the figures represent the eye guides to show the trend of the binary system.

TABLE 1: Summary of the solid phase samples before and after the immersion experiment.

System	Subsystem	Mixing molar ratio (La:Nd, La:Eu, Eu:Tm)	Crystal phase[a)]	
			Before immersion	After immersion
Binary	$(La,Nd)_2O_3$	La:Nd = 9:1~1:9	trigonal (P-3m1) single SS	hexagonal (P63/m), single SS
	La_2O_3+Nd_2O_3	La:Nd = 5:5	two separated trigonal (P-3m1)	two separated hexagonal (P63/m)
	$(La,Eu)_2O_3$	La:Eu = 9:1~1:9	trigonal (P-3m1) SS, cubic (Ia-3) SS, monoclinic (C12/m1) SS	hexagonal (P63/m) single SS
	La_2O_3+Eu_2O_3	La:Eu = 5:5	trigonal (P-3m1), cubic (Ia-3)	cubic (Ia-3), two separated hexagonal (P63/m)
	$(Eu,Tm)_2O_3$	Eu:Tm = 9:1~1:9	two separated cubic (Ia-3) SS	hexagonal (P63/m) SS, cubic (Ia-3) SS
	Eu_2O_3+Tm_2O_3	Eu:Tm = 5:5	two separated cubic (Ia-3)	hexagonal (P63/m), two separated cubic (Ia-3)
Ternary	$(La,Nd,Eu)_2O_3$	La:Nd:Eu = 4.75:4.75:0.5~3.5:3.5:3.0	trigonal (P-3m1) SS, cubic (Ia-3) SS, monoclinic (C12/m1) SS	hexagonal (P63/m) single SS
	La_2O_3+Nd_2O_3 +Eu_2O_3	La:Nd:Eu = 5:5:5	two separated trigonal (P-3m1), cubic (Ia-3)	three separated hexagonal (P63/m), cubic (Ia-3)
	$(La,Eu,Tm)_2O_3$	La:Eu:Tm = 0.5:4.75:4.75~4.5:4.5:1	trigonal (P-3m1) SS, cubic (Ia-3) SS, monoclinic (C12/m1) SS	hexagonal (P63/m) SS, cubic (Ia-3) SS
	La_2O_3+Eu_2O_3+Tm_2O_3	La:Eu:Tm = 5:5:5	trigonal (P-3m1), two separated cubic (Ia-3)	hexagonal (P63/m), two separated cubic (Ia-3)

a) SS in the table stands for solid solution.

12a shows the lattice parameter *a* and weight fraction of the hexagonal phase (P63/m) as a function of the La ratio. For both $(La,Nd)(OH)_3$ and $(La,Eu)(OH)_3$, the lattice parameter gradually increased compared to those of pure $Nd(OH)_3$ and $Eu(OH)_3$ with increasing La ratios, supporting the formation of a complete solid solution of $(La,Nd)(OH)_3$ and $(La,Eu)(OH)_3$. The ternary system $(La,Nd,Eu)_2O_3$ also resulted in the formation of a complete solid solution of the hexagonal $(La,Nd,Eu)(OH)_3$ phase. The lattice parameter determined for La:Nd:Eu = 4.75:4.75:0.5 was found to follow the trend of binary $(La,Nd)(OH)_3$ and approach that of $(La,Eu)(OH)_3$, as the Eu ratio increased up to La:Nd:Eu = 3.5:3.5:3.0. The lattice parameter of the hexagonal phase for $(La,Eu,Tm)(OH)_3$ was rather scattered; however, it seemed to be along that of the binary $(La,Eu)(OH)_3$. As discussed in the previous section, the low value of La:Eu:Tm = 4.5:4.5:1.0 may be due to the incorporation of Tm into the hexagonal phase.

Figure 12b shows the lattice parameter *a* and weight fraction of the Tm_2O_3-based cubic phase (Ia-3) as a function of the Eu ratio. By comparing the lattice parameters to those before contact with an aqueous solution in Figure 6b, hardly any change in values was noticed after aging at 60 °C for 4 weeks. Therefore, the Tm_2O_3-based cubic phase was considered to be stable, and no significant change appeared to occur in its bulk phase.

It should be noted that the lattice parameters for the solid phases after contact of $La_2O_3 + Nd_2O_3$ with an aqueous solution matched well those of pure $La(OH)_3$ and $Nd(OH)_3$, as shown in Figure 12a. This confirmed that only the $(La,Nd)_2O_3$ solid solution was transformed into the $(La,Nd)(OH)_3$ solid solution, while the separated $La_2O_3 + Nd_2O_3$ was transformed to separated $La(OH)_3 + Nd(OH)_3$. Therefore, it was suggested that the transformation of La_2O_3 or Nd_2O_3 to $La(OH)_3$ or $Nd(OH)_3$ under the investigated conditions proceeded via solid phase reactions, such as the incorporation of H_2O from the surface, that led to the conversion of the oxides to hydroxides. The low La and Nd solubilities within the neutral pH region might lead to a limited pathway of dissolution/reprecipitation to form a solid solution.

The determined lattice parameters were in good agreement with those obtained for the La-Eu binary system. These results indicate that the solid phases of the investigated ternary systems can be suitably explained based on a combination of binary systems.

Table 1 summarizes the obtained solid phases before and after contacting the aqueous phase.

4. Conclusion

Binary and ternary mixed lanthanide oxides in various proportions were synthesized and studied before and after contact with an aqueous solution using powder XRD. The XRD patterns of $(La,Nd)_2O_3$ confirmed the formation of single complete solid solutions with a trigonal phase at all mixing ratios, whereas $(La,Eu)_2O_3$ and $(Eu,Tm)_2O_3$ consisted of mixtures of different solid solutions. The formation of ternary oxides such as $(La,Nd,Eu)_2O_3$ and $(La,Eu,Tm)_2O_3$ could be well explained based on the combination of binary $(La,Nd)_2O_3$, $(La,Eu)_2O_3$, and $(Eu,Tm)_2O_3$ phases. After contact with an aqueous phase at neutral pH and 60 °C for 4 weeks, it was found that $(La,Nd)_2O_3$ and $(La,Eu)_2O_3$ were transformed into complete solid solutions of $(La,Nd)(OH)_3$ and $(La,Eu)(OH)_3$. Interestingly, a mixture of La_2O_3 and Nd_2O_3 without any heat treatment was transformed to separate $La(OH)_3$ and $Nd(OH)_3$. After contact with an aqueous phase, the ternary $(La,Nd,Eu)_2O_3$ solid solution was completely transformed into a single solid solution of $(La,Nd,Eu)(OH)_3$. $(La,Eu,Tm)_2O_3$ was also converted to $(La,Eu,Tm)(OH)_3$. The trend of the solid phase transformation of the ternary phases, including the lattice parameters tendency, was well interpreted using a combination of binary systems. Since the safety assessment of radioactive waste disposal requires a reliable prediction of radionuclides solubilities, it is important to characterize the solubility-controlling solid phase in aqueous systems. The present study on the transformation of binary and ternary lanthanide oxides in an aqueous solution after aging at an elevated temperature would be a basis for the characterization of polyvalent actinide oxide solid phases, and subsequently more complexed multicomponent solid phases in aqueous systems relevant to the radioactive waste disposal.

Acknowledgements

The authors gratefully acknowledge the financial support from the Japan Society for the Promotion of Science KAKENHI (Grant No. 20H02665).

References

[1] S. F. Marsh, *Anal. Chem.* **39**(6), 641 (1967).
[2] B.J Lewis, W.T. Thompson, F.C. Iglesias, Comprehensive Nuclear Materials 2, 515 (2012).
[3] Japan Nuclear Cycle Development Institute: 2nd progress report on research and development for the geological disposal of HLW in Japan, JNC Report TN1410 2000–001, JNC, Tokai, Japan (2000).
[4] International Atomic Energy Agency: Geological disposal of radioactive waste: technological implications for retrievability; IAEA Nuclear Energy Series No. NWT-1.19, IAEA, Vienna (2009).
[5] R. J. M. Konings and L. Gorokhov, J. Phys. Chem, 43.1 (2014).
[6] P.Brown and C.Ekberg, Hydrolysis of metal ions, Wiley-VCH, 1 (2016).
[7] S. J. Schneider and R. S. Roth, Physics and Chemistry, 64A, 4 (1960).
[8] S.Wenhui, L.Xiaoxiang, J.Mingzhi, X.Weiming, W.Dairning, and L.Milan, Phys. Rev. B, 37, p35–37 (1988).
[9] Z. Heiba, H. Okuyucus and Y. Hascicek, J. App. Crysta. 35, 577–580 (2002).
[10] T. Hirsch, R. Uecker and D.Klimm, Cryst. Res. Tech. 52, 1, 1600237 (2017).
[11] V. Bellie`re, G. Joorst, O. Stephan, F. de Groot, and B. M. Weckhuysen J. Phys. Chem. B, 110, 9984–9990 (2006).
[12] D. Horlait, N. Clavier, S. Szenknect, N. Dacheux, and V. Inorg. Chem. 51, 3868–3878 (2012).
[13] K. P. Tseng, Q. Yang, S. J. McCormack and W. M. Kriven, J. Am. Ceram Soc.103:569–576 (2020).
[14] R. Djenadic, A. Sarkar, O. Clemens, C. Loho, M. Btros, V.S.K. Chakravadhanula Bhattacharya, C. Kubel, Subramshu S, A.S. Gandhi and H. Hahn, Mater. Res. Lett., 5, 2, 102–109 (2017).
[15] O.A. Korniienko, A.I. Bykov and E.R. Andrievskaya, Powder Metallurgy and Metal Ceramics, 59, 3–4 (2020).
[16] J. C. Soares, K.P.F. Siqueira, R.L. Moreira and A. Dias, Arabian J. Chem. 12, 4035–4043 (2019).
[17] I. I. Diakonov, B. R. Tagirov and K. V. Ragnarsdottir, Radiochim. Acta 81, 107–116 (1998).
[18] I. I. Diakonov, K.V. Ragnarsdottir and B.R. Tagirov, Chem. Geol. 151, 327–347(1998).
[19] M. Moniruzzaman, T. Kobayashi and T. Sasaki, J. Nucl. Radiochem. Sci, Vol. 20, 32–42 (2020).
[20] M. H. Nguyen, S. J. Lee, and W. M. Kriven, J. Mat. Res. 14, 3417–3426 (1999).
[21] M.A. Gulgun, M. H. Nguyen and W.M. Kriven, J. Am. Ceram. Soc., 82, 3, 556–60 (1999).
[22] A. Navrotsky, W. Lee, A. Mielewczyk-Gryn, S.V.

Ushakov, H. Wu and R. E. Riman, J. Chem. Thermodyna, 88, 126–141 (2015).
[23] M. Zinkevich, Progress in Materials Science, 52, 97–647 (2007).
[24] V. Neck, M. Altmaier, T. Rabung, J. Lützenkirchen and T. Fanghänel, Pure Appl. Chem., 81, 9, 1555–1568 (2009).

Appendix

TABLE A1. Summary of the Rietveld analysis of the La-Nd binary solid phases before and after contact with the sample solution**.**

Sample	Mixing ratio La/La+Nd	Crystal phase	Weight fraction of crystal phase	Lattice parameter a(Å)	b(Å)	c(Å)	R-factor Rwp	Rp	S
before the solubility experiment									
La_2O_3	1	Trigonal P-3m1(164)	1.00	3.93997(9)	3.93997(9)	6.13380(14)	0.165	0.106	2.183
LN91	0.9		1.00	3.93374(13)	3.93374(13)	6.1282(2)	0.232	0.163	3.160
LN73	0.7		1.00	3.91685(17)	3.91685(17)	6.1065(3)	0.163	0.118	2.327
LN55	0.5		1.00	3.89332(19)	3.89332(19)	6.0764(4)	0.166	0.121	2.548
LN46	0.4		1.00	3.8839(3)	3.8839(3)	6.0640(6)	0.184	0.137	2.881
LN37	0.3		1.00	3.8529(3)	3.8529(3)	6.0226(5)	0.179	0.130	2.833
LN19	0.1		1.00	3.83675(15)	3.83675(15)	6.0049(3)	0.184	0.127	3.067
Nd_2O_3	0		1.00	3.83310(6)	3.83310(6)	6.00381(10)	0.130	0.089	2.139
La_2O_3 + Nd_2O_3	0.5		0.49	3.93909(4)	3.93909(4)	6.13361(7)	0.0654	0.0488	1.037
			0.51	3.83220(4)	3.83220(4)	6.00089(7)			
after the solubility experiment									
LN91	0.9	Hexagonal P63/m(176)	1.00	6.5333(7)	6.5333(7)	3.8492(4)	0.258	0.195	3.183
LN73	0.7		1.00	6.4904(2)	6.4904(2)	3.81315(15)	0.114	0.090	1.756
LN55	0.5		1.00	6.4749(6)	6.4749(6)	3.7940(4)	0.171	0.131	2.277
LN46	0.4		1.00	6.4564(10)	6.4564(10)	3.7793(6)	0.181	0.136	2.384
LN37	0.3		1.00	6.4406(7)	6.4406(7)	3.7614(5)	0.188	0.135	2.888
LN19	0.1		1.00	6.42609(17)	6.42609(17)	3.74253(13)	0.101	0.075	1.439
La_2O_3 + Nd_2O_3	0.5		1.00	6.5216(6)	6.5216(6)	3.8494(4)	0.110	0.083	1.545
			1.00	6.4152(6)	6.4152(6)	3.7315(4)			

TABLE A2. Summary of the Rietveld analysis of the La-Eu binary solid phases before and after contact with the sample solution.

Sample	Mixing ratio	Crystal phase	Weight fraction of crystal phase	Lattice parameter			R-factor		
	La/La+Eu			a(Å)	b(Å)	c(Å)	Rwp	Rp	S
before the solubility experiment									
La_2O_3	1	Trigonal P-3m1(164)	1.00	3.93997(9)	3.93997(9)	6.13380(14)	0.165	0.106	2.183
LE91	0.9	Trigonal P-3m1(164)	1.00	3.92971(14)	3.92971(14)	6.1225(3)	0.178	0.120	2.771
LE73	0.7	Trigonal P-3m1(164)	0.79	3.9272(4)	3.9272(4)	6.1184(7)	0.132	0.089	2.448
		Cubic Ia-3(206)	0.21	10.924(4)	10.924(4)	10.924(4)			
LE55	0.5	Trigonal P-3m1(164)	0.31	3.8678(5)	3.8678(5)	6.0540(9)	0.056	0.039	1.137
		Cubic Ia-3(206)	0.06	10.884(2)	10.884(2)	10.884(2)			
		Monoclinic C12/m1(12)	0.63	14.373(2)	3.6989(5)	8.9968(13)			
LE46	0.4	Trigonal P-3m1(164)	0.17	3.8688(13)	3.8688(13)	6.060(2)	0.055	0.037	1.191
		Cubic Ia-3(206)	0.20	10.883(2)	10.883(2)	10.883(2)			
		Monoclinic C12/m1(12)	0.64	14.354(3)	3.6893(8)	8.9785(18)			
LE37	0.3	Trigonal P-3m1(164)	0.20	3.8691(11)	3.8691(11)	6.062(3)	0.121	0.092	2.471
		Cubic Ia-3(206)	0.26	10.895(3)	10.895(3)	10.895(3)			
		Monoclinic C12/m1(12)	0.54	14.310(6)	3.6668(16)	8.939(4)			
LE19	0.1	Trigonal (P-3m1(164))	0.23	3.9306(8)	3.9306(8)	6.1184(16)	0.111	0.077	2.392
		Cubic Ia-3(206)	0.39	10.8915(14)	10.8915(14)	10.8915(14)			
		Monoclinic C12/m1(12)	0.38	14.171(12)	3.700(3)	8.947(9)			
Eu_2O_3	1	Cubic Ia-3(206)	1.00	10.8755(2)	10.8755(2)	10.8755(2)	0.074	0.047	2.011
La_2O_3 + Eu_2O_3	0.5	Trigonal (P-3m1(164))	0.45	3.94036(12)	3.94036(12)	6.1357(2)	0.088	0.051	1.801
		Cubic Ia-3(206)	0.55	10.8761(4)	10.8761(4)	10.8761(4)			
after the solubility experiment									
LE91	0.9	Hexagonal P63/m(176)	1.00	6.5143(5)	6.5143(5)	3.8379(3)	0.182	0.133	2.538
LE73	0.7		1.00	6.4937(6)	6.4937(6)	3.8236(4)	0.102	0.080	1.752
LE55	0.5		1.00	6.4260(7)	6.4260(7)	3.7427(4)	0.094	0.069	1.792
LE46	0.4		1.00	6.4334(5)	6.4334(5)	3.7391(3)	0.049	0.037	1.131
LE37	0.3		1.00	6.4028(5)	6.4028(5)	3.7097(3)	0.046	0.036	1.096
LE19	0.1		1.00	6.3762(12)	6.3762(12)	3.6827(7)	0.073	0.053	1.524
La_2O_3 + Eu_2O_3	0.5	Hexagonal P63/m(176)	0.54	6.5372(7)	6.5372(7)	3.8573(5)	0.074	0.057	1.455
			0.11	6.361(3)	6.361(3)	3.6615(16)			
		Cubic Ia-3(206)	0.35	11.333(7)	11.333(7)	11.333(7)			

TABLe A3. Summary of the Rietveld analysis of the Eu-Tm binary solid phases before and after contact with the sample solution.

Sample	Mixing ratio	Crystal phase	Weight fraction of crystal phase	Lattice parameter			R-factor		
	Eu/Eu+Tm			a(Å)	b(Å)	c(Å)	Rwp	Rp	S
before the solubility experiment									
Eu_2O_3	1	Cubic Ia-3(206)	1.00	10.8755(2)	10.8755(2)	10.8755(2)	0.074	0.047	2.011
ET91	0.9	Cubic Ia-3(206)	1.00	10.8495(4)	10.8495(4)	10.8495(4)	0.067	0.041	1.699
ET73	0.7	Cubic Ia-3(206)	0.62	10.8346(11)	10.8346(11)	10.8346(11)	0.051	0.034	1.182
		Cubic Ia-3(206)	0.38	10.6453(10)	10.6453(10)	10.6453(10)			
ET55	0.5	Cubic Ia-3(206)	0.49	10.8297(8)	10.8297(8)	10.8297(8)	0.063	0.043	1.425
		Cubic Ia-3(206)	0.51	10.5819(5)	10.5819(5)	10.5819(5)			
ET46	0.4	Cubic Ia-3(206)	0.20	10.768(3)	10.768(3)	10.768(3)	0.078	0.056	1.529
		Cubic Ia-3(206)	0.80	10.5891(10)	10.5891(10)	10.5891(10)			
ET37	0.3	Cubic Ia-3(206)	0.34	10.7093(15)	10.7093(15)	10.7093(15)	0.085	0.058	1.772
		Cubic Ia-3(206)	0.66	10.6054(14)	10.6054(14)	10.6054(14)			
ET19	0.1	Cubic Ia-3(206)	1.00	10.5296(4)	10.5296(4)	10.5296(4)	0.080	0.058	1.830
Tm_2O_3	0	Cubic Ia-3(206)	1.00	10.49207(17)	10.49207(17)	10.49207(17)	0.052	0.039	1.637
Eu_2O_3 + Tm_2O_3	0.5	Cubic Ia-3(206)	0.39	10.8777(3)	10.8777(3)	10.8777(3)	0.052	0.037	1.485
		Cubic Ia-3(206)	0.61	10.49316(14)	10.49316(14)	10.49316(14)			
after the solubility experiment									
ET91	0.9	Hexagonal P63/m(176)	1.00	6.3452(3)	6.3452(3)	3.63678(19)	0.045	0.034	1.122
ET73	0.7	Hexagonal P63/m(176)	0.38	6.3478(6)	6.3478(6)	3.6308(5)	0.053	0.039	1.447
		Cubic Ia-3(206)	0.62	10.6695(11)	10.6695(11)	10.6695(11)			
ET55	0.5	Hexagonal P63/m(176)	0.13	6.319(3)	6.319(3)	3.674(2)	0.047	0.035	1.168
		Cubic Ia-3(206)	0.87	10.5641(10)	10.5641(10)	10.5641(10)			
ET46	0.4	Cubic Ia-3(206)	1.00	10.5675(8)	10.5675(8)	10.5675(8)	0.064	0.046	1.211
ET37	0.3	Cubic Ia-3(206)	1.00	10.5469(7)	10.5469(7)	10.5469(7)	0.054	0.041	1.295
ET19	0.1	Cubic Ia-3(206)	1.00	10.5383(6)	10.5383(6)	10.5383(6)	0.106	0.078	2.419
Eu_2O_3 + Tm_2O_3	0.5	Hexagonal P63/m(176)	0.23	6.336(7)	6.336(7)	3.299(6)	0.058	0.045	1.639
		Cubic Ia-3(206)	0.45	10.944(6)	10.944(6)	10.944(6)			
		Cubic Ia-3(206)	0.32	10.4988(4)	10.4988(4)	10.4988(4)			

TABLE A4. Summary of the Rietveld analysis of the La-Nd-Eu ternary solid phases before and after contact with the sample solution.

Sample	Mixing ratio			Crystal phase	Weight fraction of crystal phase	Lattice parameter			R-factor		
	La	Nd	Eu			a(Å)	b(Å)	c(Å)	Rwp	Rp	S
before the solubility experiment											
LNE-1	0.475	0.475	0.05	Trigonal P-3m1(164)	1.00	3.88810(17)	3.88810(17)	6.0758(3)	0.137	0.096	1.906
LNE-2	0.45	0.45	0.1	Trigonal P-3m1(164)	0.99	3.87403(17)	3.87403(17)	6.0561(3)	0.084	0.061	1.246
				Cubic Ia-3(206)	0.01	11.308(10)	11.308(10)	11.308(10)			
LNE-3	0.35	0.35	0.3	Trigonal P-3m1(164)	0.46	3.8543(3)	3.8543(3)	6.0359(6)	0.055	0.041	0.974
				Cubic Ia-3(206)	0.03	10.974(4)	10.974(4)	10.974(4)			
				Monoclinic C12/m1(12)	0.51	14.3294(15)	3.6894(4)	8.9723(10)			
La_2O_3 + Nd_2O_3 + Eu_2O_3	0.33	0.33	0.33	Trigonal P-3m1(164)	0.32	3.93890(13)	3.93890(13)	6.1337(3)	0.129	0.089	2.517
				Trigonal P-3m1(164)	0.27	3.83288(18)	3.83288(18)	6.0020(3)			
				Cubic Ia-3(206)	0.41	10.8705(2)	10.8705(2)	10.8705(2)			
after the solubility experiment											
LNE-1	0.475	0.475	0.05	Hexagonal P63/m(176)	1.00	6.4687(3)	6.4687(3)	3.78469(17)	0.119	0.090	1.795
LNE-2	0.45	0.45	0.1	Hexagonal P63/m(176)	1.00	6.4585(2)	6.4585(2)	3.77479(14)	0.099	0.076	1.629
LNE-3	0.35	0.35	0.3	Hexagonal P63/m(176)	1.00	6.4280(3)	6.4280(3)	3.7401(2)	0.100	0.072	1.717
La_2O_3 + Nd_2O_3 + Eu_2O_3	0.33	0.33	0.33	Hexagonal P63/m(176)	0.35	6.5344(8)	6.5344(8)	3.8622(5)	0.231	0.260	1.062
				Hexagonal P63/m(176)	0.23	6.4335(11)	6.4335(11)	3.7468(8)			
				Hexagonal P63/m(176)	0.21	6.424(2)	6.424(2)	3.6813(13)			
				Cubic Ia-3(206)	0.22	10.83(3)	10.83(3)	10.83(3)			

TABLE A5. Summary of the Rietveld analysis of the La-Eu-Tm ternary solid phases before and after contact with the sample solution.

Sample	Mixing ratio			Crystal phase	Weight fraction of crystal phase	Lattice parameter			R-factor		
	La	Eu	Tm			a(Å)	b(Å)	c(Å)	Rwp	Rp	S
before the solubility experiment											
LET-1	0.05	0.475	0.475	Cubic Ia-3(206)	0.62	10.8312(15)	10.8312(15)	10.8312(15)	0.052	0.033	1.264
				Cubic Ia-3(206)	0.38	10.6367(11)	10.6367(11)	10.6367(11)			
LET-2	0.1	0.45	0.45	Cubic Ia-3(206)	0.56	10.8455(13)	10.8455(13)	10.8455(13)	0.047	0.033	1.111
				Cubic Ia-3(206)	0.44	10.6111(12)	10.6111(12)	10.6111(12)			
LET-3	0.3	0.35	0.35	Trigonal P-3m1(164)	0.30	3.9027(15)	3.9027(15)	6.113(3)	0.105	0.073	2.282
				Cubic Ia-3(206)	0.16	10.867(2)	10.867(2)	10.867(2)			
LET-4	0.45	0.45	0.1	Cubic Ia-3(206)	0.54	10.632(2)	10.632(2)	10.632(2)	0.103	0.066	1.847
				Trigonal P-3m1(164)	0.14	3.9016(11)	3.9016(11)	6.095(2)			
				Cubic Ia-3(206)	0.19	10.813(2)	10.813(2)	10.813(2)			
				Monoclinic C12/m1(12)	0.67	14.377(6)	3.6821(13)	8.976(4)			
La_2O_3 + Eu_2O_3 + Tm_2O_3	0.33	0.33	0.33	Trigonal P-3m1(164)	0.26	3.94100(13)	3.94100(13)	6.1367(2)	0.099	0.059	2.293
				Cubic Ia-3(206)	0.34	10.8782(4)	10.8782(4)	10.8782(4)			
				Cubic Ia-3(206)	0.40	10.4994(2)	10.4994(2)	10.4994(2)			
after the solubility experiment											
LET-1	0.05	0.475	0.475	Hexagonal P63/m(176)	0.23	6.396(4)	6.396(4)	3.582(2)	0.062	0.045	0.984
				Cubic Ia-3(206)	0.77	10.618(2)	10.618(2)	10.618(2)			
LET-2	0.1	0.45	0.45	Hexagonal P63/m(176)	0.35	6.3443(8)	6.3443(8)	3.6280(5)	0.043	0.034	1.060
				Cubic Ia-3(206)	0.65	10.5832(12)	10.5832(12)	10.5832(12)			
LET-3	0.3	0.35	0.35	Hexagonal P63/m(176)	0.38	6.444(2)	6.444(2)	3.7175(15)	0.118	0.083	2.554
				Cubic Ia-3(206)	0.62	10.575(2)	10.575(2)	10.575(2)			
LET-4	0.45	0.45	0.1	Hexagonal P63/m(176)	0.98	6.4199(7)	6.4199(7)	3.7211(4)	0.063	0.048	1.457
				Cubic Ia-3(206)	0.02	10.552(3)	10.552(3)	10.552(3)			
La_2O_3 + Eu O + Tm_2O_3	0.33	0.33	0.33	Hexagonal P63/m(176)	0.37	6.5306(5)	6.5306(5)	3.8572(4)	0.096	0.070	2.207
				Cubic Ia-3(206)	0.16	10.8750(15)	10.8750(15)	10.8750(15)			
				Cubic Ia-3(206)	0.48	10.4857(2)	10.4857(2)	10.4857(2)			